Approaches for high internal quantum efficiency green InGaN light-emitting diodes with large overlap quantum wells

Hongping Zhao,[1,3,4] Guangyu Liu,[1] Jing Zhang,[1] Jonathan D. Poplawsky,[2] Volkmar Dierolf,[2] and Nelson Tansu[1,5]

[1]*Center for Optical Technologies, Department of Electrical and Computer Engineering, Lehigh University, Bethlehem, Pennsylvania 18015, USA*
[2]*Department of Physics, Center for Optical Technologies, Lehigh University, Bethlehem, Pennsylvania 18015, USA*
[3]*Department of Electrical Engineering and Computer Science, Case Western Reserve University, Cleveland, Ohio 44106, USA*
[4]*hongping.zhao@case.edu*
[5]*tansu@lehigh.edu*

Abstract: Optimization of internal quantum efficiency (IQE) for InGaN quantum wells (QWs) light-emitting diodes (LEDs) is investigated. Staggered InGaN QWs with large electron-hole wavefunction overlap and improved radiative recombination rate are investigated for nitride LEDs application. The effect of interface abruptness in staggered InGaN QWs on radiative recombination rate is studied. Studies show that the less interface abruptness between the InGaN sub-layers will not affect the performance of the staggered InGaN QWs detrimentally. The growths of linearly-shaped staggered InGaN QWs by employing graded growth temperature grading are presented. The effect of current injection efficiency on IQE of InGaN QWs LEDs and other approaches to reduce dislocation in InGaN QWs LEDs are also discussed. The optimization of both radiative efficiency and current injection efficiency in InGaN QWs LEDs are required for achieving high IQE devices emitting in the green spectral regime and longer.

©2011 Optical Society of America

OCIS codes: (230.3670) Light-emitting diodes; (230.0250) Optoelectronics; (040.4200) Multiple quantum well.

References and links

1. M. H. Crawford, “LEDs for solid-state lighting: performance challenges and recent advances,” IEEE J. Sel. Top. Quantum Electron. **15**(4), 1028–1040 (2009).
2. D. D. Koleske, A. J. Fischer, A. A. Allerman, C. C. Mitchell, K. C. Cross, S. R. Kurtz, J. J. Figiel, K. W. Fullmer, and W. G. Breiland, “Improved brightness of 380 nm GaN light emitting diodes through intentional delay of the nucleation island coalescence,” Appl. Phys. Lett. **81**(11), 1940–1942 (2002).
3. J. Han and A. V. Nurmikko, “Advances in AlGaInN blue and ultraviolet light emitters,” IEEE J. Sel. Top. Quantum Electron. **8**(2), 289–297 (2002).
4. M. Kneissl, D. W. Treat, M. Teepe, N. Miyashita, and N. M. Johnson, “Continuous-wave operation of ultraviolet InGaN/InAlGaN multiple-quantum-well laser diodes,” Appl. Phys. Lett. **82**(15), 2386–2388 (2003).
5. D. Queren, A. Avramescu, G. Brüderl, A. Breidenassel, M. Schillgalies, S. Lutgen, and U. Strauß, “500 nm electrically driven InGaN based laser diodes,” Appl. Phys. Lett. **94**(8), 081119 (2009).
6. K. Okamoto and Y. Kawakami, “High-efficiency InGaN/GaN light emitters based on nanophotonics and plasmonics,” IEEE J. Sel. Top. Quantum Electron. **15**(4), 1199–1209 (2009).
7. H. Zhao, J. Zhang, G. Liu, and N. Tansu, “Surface plasmon dispersion engineering via double-metallic Au/Ag layers for III-nitride based light-emitting diodes,” Appl. Phys. Lett. **98**(15), 151115 (2011).
8. J. Henson, A. Bhattacharyya, T. D. Moustakas, and R. Paiella, “Controlling the recombination rate of semiconductor active layers via coupling to dispersion-engineered surface plasmons,” J. Opt. Soc. Am. B **25**(8), 1328–1335 (2008).
9. X. Li, S. Kim, E. E. Reuter, S. G. Bishop, and J. J. Coleman, “The incorporation of arsenic in GaN by metalorganic chemical vapor deposition,” Appl. Phys. Lett. **72**(16), 1990–1992 (1998).
10. T. Jung, L. K. Lee, and P.-C. Ku, “Novel epitaxial nanostructures for the improvement of InGaN LEDs efficiency,” IEEE J. Sel. Top. Quantum Electron. **15**(4), 1073–1079 (2009).
11. X. Li, S. G. Bishop, and J. J. Coleman, “GaN epitaxial lateral overgrowth and optical characterization,” Appl. Phys. Lett. **73**(9), 1179–1181 (1998).

#147902 - $15.00 USD
Received 19 May 2011; accepted 22 Jun 2011; published 1 Jul 2011
(C) 2011 OSA

12. J. Liu, J. Limb, Z. Lochner, D. Yoo, J.-H. Ryou, and R. D. Dupuis, "Green light-emitting diodes with p-InGaN:Mg grown on C-plane sapphire and GaN substrates," Phys. Status Solidi., A Appl. Mater. Sci. **206**(4), 750–753 (2009).
13. W. Lee, J. Limb, J.-H. Ryou, D. Yoo, M. A. Ewing, Y. Korenblit, and R. D. Dupuis, "Nitride-based green light-emitting diodes with various p-type layers," J. Disp. Technol. **3**(2), 126–132 (2007).
14. G. R. Mutta, P. Ruterana, J. L. Doualan, M. P. Chauvat, F. Ivaldi, S. Kret, N. A. K. Kaufmann, A. Dussaigne, D. Martin, and N. Grandjean, "Investigation of the In composition in InGaN/GaN quantum wells deposited by MOVPE and/or MBE with emission from violet to green," Phys. Status Solidi, B Basic Res. **248**(5), 1187–1190 (2011).
15. C. H. Chao, S. L. Chuang, and T. L. Wu, "Theoretical demonstration of enhancement of light extraction of flip-chip GaN light-emitting diodes with photonic crystals," Appl. Phys. Lett. **89**(9), 091116 (2006).
16. K. McGroddy, A. David, E. Matioli, M. Iza, S. Nakamura, S. DenBaars, J. S. Speck, C. Weisbuch, and E. L. Hu, "Directional emission control and increased light extraction in GaN photonic crystal light emitting diodes," Appl. Phys. Lett. **93**(10), 103502 (2008).
17. J. J. Wierer, A. David, and M. M. Megens, "III-nitride photonic-crystal light-emitting diodes with high extraction efficiency," Nat. Photonics **3**(3), 163–169 (2009).
18. X. H. Li, R. Song, Y. K. Ee, P. Kumnorkaew, J. F. Gilchrist, and N. Tansu, "Light extraction efficiency and radiation patterns of III-nitride light-emitting diodes with colloidal microlens arrays with various aspect ratios," IEEE Photon. J. **3**(3), 489–499 (2011).
19. Q. Xi, M. F. Schubert, J. K. Kim, E. F. Schubert, M. Chen, S. Y. Lin, W. Liu, and J. A. Smart, "Optical thin-film materials with low refractive index for broadband elimination of fresnel reflection," Nat. Photonics **1**, 176–179 (2007).
20. S. Chhajed, W. Lee, J. Cho, E. F. Schubert, and J. K. Kim, "Strong light extraction enhancement in GaInN light-emitting diodes by using self-organized nanoscale patterning of p-type GaN," Appl. Phys. Lett. **98**(7), 071102 (2011).
21. U. K. Mishra, P. Parikh, and Y. F. Wu, "AlGaN/GaN HEMTs-an overview of device operation and applications," Proc. IEEE **90**(6), 1022–1031 (2002).
22. B. N. Pantha, R. Dahal, J. Li, J. Y. Lin, H. X. Jiang, and G. Pomrenke, "Thermoelectric properties of $In_xGa_{1-x}N$ alloys," Appl. Phys. Lett. **92**(4), 042112 (2008).
23. J. Zhang, H. Tong, G. Y. Liu, J. A. Herbsommer, G. S. Huang, and N. Tansu, "Characterizations of seebeck coefficients and thermoelectric figures of merit for AlInN alloys with various in-contents," J. Appl. Phys. **109**(5), 053706 (2011).
24. R. Dahal, B. Pantha, J. Li, J. Y. Lin, and H. X. Jiang, "InGaN/GaN multiple quantum well solar cells with long operating wavelengths," Appl. Phys. Lett. **94**(6), 063505 (2009).
25. C. J. Neufeld, N. G. Toledo, S. C. Cruz, M. Iza, S. P. DenBaars, and U. K. Mishra, "High quantum efficiency InGaN/GaN solar cells with 2.95 eV band gap," Appl. Phys. Lett. **93**(14), 143502 (2008).
26. O. Jani, I. Ferguson, C. Honsberg, and S. Kurtz, "Design and characterization of GaN/InGaN solar cells," Appl. Phys. Lett. **91**(13), 132117 (2007).
27. Z. H. Wu, A. M. Fischer, F. A. Ponce, W. Lee, J. H. Ryou, J. Limb, D. Yoo, and R. D. Dupuis, "Effect of internal electrostatic fields in InGaN quantum wells on the properties of green light emitting diodes," Appl. Phys. Lett. **91**(4), 041915 (2007).
28. S. H. Park and S. L. Chuang, "Spontaneous polarization effects in wurtzite GaN/AlGaN quantum wells and comparison with experiment," Appl. Phys. Lett. **76**(15), 1981–1983 (2000).
29. S. H. Park and S. L. Chuang, "Comparison of zinc-blende and wurtzite GaN semiconductors with spontaneous polarization and piezoelectric field effects," J. Appl. Phys. **87**(1), 353–364 (2000).
30. S. H. Park and S. L. Chuang, "Crystal-orientation effects on the piezoelectric field and electronic properties of strained wurtzite semiconductors," Phys. Rev. B **59**(7), 4725–4737 (1999).
31. S. H. Park and S. L. Chuang, "Crystal orientation dependence of many-body optical gain in wurtzite GaN/AlGaN quantum-well lasers," Semicond. Sci. Technol. **17**(7), 686–691 (2002).
32. T. Takeuchi, H. Amano, and I. Akasaki, "Theoretical study of orientation dependence of piezoelectric effects in wurtzite strained GaInN/GaN heterostructures and quantum wells," Jpn. J. Appl. Phys. **39**(Part 1, No. 2A), 413–416 (2000).
33. I. H. Brown, P. Blood, P. M. Smowton, J. D. Thomson, S. M. Olaizola, A. M. Fox, P. J. Parbrook, and W. W. Chow, "Time evolution of the screening of piezoelectric fields in InGaN quantum wells," IEEE J. Quantum Electron. **42**(12), 1202–1208 (2006).
34. I. Vurgaftman and J. R. Meyer, "Band parameters for nitrogen-containing semiconductors," J. Appl. Phys. **94**(6), 3675–3696 (2003).
35. U. T. Schwarz, H. Braun, K. Kojima, Y. Kawakami, S. Nagahama, and T. Mukai, "Interplay of built-in potential and piezoelectric field on carrier recombination in green light emitting InGaN quantum wells," Appl. Phys. Lett. **91**(12), 123503 (2007).
36. A. Venkatachalam, B. Klein, J.-H. Ryou, S. C. Shen, R. D. Dupuis, and P. D. Yoder, "Design strategies for InGaN-based green lasers," IEEE J. Quantum Electron. **46**(2), 238–245 (2010).
37. J.-H. Ryou, P. D. Yoder, J. Liu, Z. Lochner, H. Kim, S. Choi, H. J. Kim, and R. D. Dupuis, "Control of quantum-confined stark effect in InGaN-based quantum wells," IEEE J. Sel. Top. Quantum Electron. **15**(4), 1080–1091 (2009).
38. T. Li, A. M. Fischer, Q. Y. Wei, F. A. Ponce, T. Detchprohm, and C. Wetzel, "Carrier localization and nonradiative recombination in yellow emitting InGaN quantum wells," Appl. Phys. Lett. **96**(3), 031906 (2010).

#147902 - $15.00 USD Received 19 May 2011; accepted 22 Jun 2011; published 1 Jul 2011
(C) 2011 OSA

39. M. Zhu, S. You, T. Detchprohm, T. Paskova, E. A. Preble, and C. Wetzel, “Various misfit dislocations in green and yellow GaInN GaN light emitting diodes,” Phys. Status Solidi., A Appl. Mater. Sci. **207**(6), 1305–1308 (2010).
40. T. Detchprohm, Y. Xia, Y. Xi, M. Zhu, W. Zhao, Y. Li, E. F. Schubert, L. Liu, D. Tsvetkov, D. Hanser, and C. Wetzel, “Dislocation analysis in homoepitaxial GaInN/GaN light emitting diode growth,” J. Cryst. Growth **298**, 272–275 (2007).
41. Y. Li, S. You, M. Zhu, L. Zhao, W. Hou, T. Detchprohm, Y. Taniguchi, N. Tamura, S. Tanaka, and C. Wetzel, “Defect-reduced green GaInN/GaN light-emitting diode on nanopatterned sapphire,” Appl. Phys. Lett. **98**(15), 151102 (2011).
42. Y. K. Ee, J. M. Biser, W. Cao, H. M. Chan, R. P. Vinci, and N. Tansu, “Metalorganic vapor phase epitaxy of III-nitride light-emitting diodes on nano-patterned AGOG sapphire substrate by abbreviated growth mode,” IEEE J. Sel. Top. Quantum Electron. **15**(4), 1066–1072 (2009).
43. S. H. Park, D. Ahn, and S. L. Chuang, “Electronic and optical properties of a- and m-plane wurtzite InGaN/GaN quantum wells,” IEEE J. Quantum Electron. **43**(12), 1175–1182 (2007).
44. M. C. Schmidt, K.-C. Kim, R. M. Farrell, D. F. Feezell, D. A. Cohen, M. Saito, K. Fujito, J. S. Speck, S. P. Denbaars, and S. Nakamura, “Demonstration of nonpolar m-plane InGaN/GaN laser diodes,” Jpn. J. Appl. Phys. **46**(9), L190–L191 (2007).
45. R. M. Farrell, D. F. Feezell, M. C. Schmidt, D. A. Haeger, K. M. Kelchner, K. Iso, H. Yamada, M. Saito, K. Fujito, D. A. Cohen, J. S. Speck, S. P. DenBaars, and S. Nakamura, “Continuous-wave operation of AlGaN-cladding-free nonpolar m-plane InGaN/GaN laser diodes,” Jpn. J. Appl. Phys. **46**(32), L761–L763 (2007).
46. R. A. Arif, Y. K. Ee, and N. Tansu, “Polarization engineering via staggered InGaN quantum wells for radiative efficiency enhancement of light emitting diodes,” Appl. Phys. Lett. **91**(9), 091110 (2007).
47. H. Zhao, R. A. Arif, and N. Tansu, “Design analysis of staggered InGaN quantum wells light-emitting diodes at 500-540 nm,” IEEE J. Sel. Top. Quantum Electron. **15**(4), 1104–1114 (2009).
48. H. P. Zhao, G. Y. Liu, X. H. Li, R. A. Arif, G. S. Huang, J. D. Poplawsky, S. Tafon Penn, V. Dierolf, and N. Tansu, “Design and characteristics of staggered InGaN quantum wells light-emitting diodes in the green spectral regimes,” IET Optoelectron. **3**(6), 283–295 (2009).
49. H. Zhao, G. Liu, X.-H. Li, G. S. Huang, J. D. Poplawsky, S. T. Penn, V. Dierolf, and N. Tansu, “Growths of staggered InGaN quantum wells light-emitting diodes emitting at 520-525 nm employing graded growth-temperature profile,” Appl. Phys. Lett. **95**(6), 061104 (2009).
50. S. H. Park, D. Ahn, and J. W. Kim, “High-efficiency Staggered 530 nm InGaN/InGaN/gan quantum-well light-emitting diodes,” Appl. Phys. Lett. **94**(4), 041109 (2009).
51. S. H. Park, D. Ahn, B. H. Koo, and J. W. Kim, “Electronic and optical properties of staggered InGaN/InGaN quantum-well light-emitting diodes,” Phys. Status Solidi., A Appl. Mater. Sci. **206**(11), 2637–2640 (2009).
52. S. H. Yen and Y. K. Kuo, “Improvement in piezoelectric effect of violet InGaN laser diodes,” Opt. Commun. **281**(18), 4735–4740 (2008).
53. S. H. Park, D. Ahn, B. H. Koo, and J. W. Kim, “Dip-shaped InGaN/GaN quantum-well light-emitting diodes with high efficiency,” Appl. Phys. Lett. **95**(6), 063507 (2009).
54. C. T. Liao, M. C. Tsai, B. T. Liou, S. H. Yen, and Y. K. Kuo, “Improvement in output power of a 460 nm InGaN light-emitting diode using staggered quantum well,” J. Appl. Phys. **108**(6), 063107 (2010).
55. H. Zhao and N. Tansu, “Optical gain characteristics of staggered InGaN quantum well lasers,” J. Appl. Phys. **107**(11), 113110 (2010).
56. S. H. Park, Y. T. Moon, J. S. Lee, H. K. Kwon, J. S. Park, and D. Ahn, “Spontaneous emission rate of green strain-compensated InGaN/InGaN LEDs using InGaN substrate,” Phys. Status Solidi., A Appl. Mater. Sci. **208**(1), 195–198 (2011).
57. H. M. Lu and G. X. Chen, “Design strategies for mitigating the influence of polarization effects on GaN-based multiple quantum well light-emitting diodes,” J. Appl. Phys. **109**(9), 093102 (2011).
58. M. C. Tsai, S. H. Yen, and Y. K. Kuo, “Investigation of blue InGaN light-emitting diodes with step-like quantum well,” Appl. Phys., A Mater. Sci. Process. **104**, (2011), doi:10.1007/s00339-011-6458-1.
59. J. Park and Y. Kawakami, “Photoluminescence property of InGaN Single quantum well with embedded AlGaN δ layer,” Appl. Phys. Lett. **88**(20), 202107 (2006).
60. S. H. Park, J. Park, and E. Yoon, “Optical gain in InGaN/GaN quantum well structures with embedded AlGaN delta layer,” Appl. Phys. Lett. **90**(2), 023508 (2007).
61. H. Zhao, R. A. Arif, and N. Tansu, “Self consistent analysis of type-II 'W' InGaN-GaNAs quantum well lasers,” J. Appl. Phys. **104**(4), 043104 (2008).
62. S. H. Park, Y. T. Lee, and J. Park, “Optical properties of type-II InGaN/GaAsN/GaN quantum wells,” Opt. Quantum Electron. **41**(11-13), 779–785 (2009).
63. S. H. Park, D. Ahn, B. H. Koo, and J. E. Oh, “Optical gain improvement in type-II InGaN/GaNSb/GaN quantum well structures composed of InGaN and GaNSb layers,” Appl. Phys. Lett. **96**(5), 051106 (2010).
64. H. Zhao, G. Liu, and N. Tansu, “Analysis of InGaN-delta-InN quantum wells for light-emitting diodes,” Appl. Phys. Lett. **97**(13), 131114 (2010).
65. Z. Yang, R. Li, Q. Wei, T. Yu, Y. Zhang, W. Chen, and X. Hu, “Analysis of optical gain property in the InGaN/GaN triangular shaped quantum well under the piezoelectric field,” Appl. Phys. Lett. **94**(6), 061120 (2009).
66. H. Zhao, R. A. Arif, Y. K. Ee, and N. Tansu, “Self-consistent analysis of strain-compensated InGaN-AlGaN quantum wells for lasers and light emitting diodes,” IEEE J. Quantum Electron. **45**(1), 66–78 (2009).
67. C. L. Tsai, G. C. Fan, and Y. S. Lee, “Effects of strain-compensated AlGaN/InGaN superlattice barriers on the optical properties of InGaN light-emitting diodes,” Appl. Phys., A Mater. Sci. Process. **104**(1), 319–323 (2011).

#147902 - $15.00 USD Received 19 May 2011; accepted 22 Jun 2011; published 1 Jul 2011
(C) 2011 OSA

68. C. R. Hall, L. V. Dao, K. Koike, S. Sasa, H. H. Tan, M. Inoue, M. Yano, C. Jagadish, and J. A. Davis, "Using graded barriers to control the optical properties of $ZnO/Zn_{0.7}Mg_{0.3}O$ quantum wells with an intrinsic internal electric field," Appl. Phys. Lett. **96**(19), 193117 (2010).
69. H. P. D. Schenk, M. Leroux, and P. de Mierry, "Luminescence and absorption in InGaN epitaxial layers and the Van Roosbroeck–Shockley relation," J. Appl. Phys. **88**(3), 1525–1534 (2000).
70. M. A. Caro, S. Schulz, S. B. Healy, and E. P. O'Reilly, "Built-in field control in alloyed c-plane III-N quantum dots and wells," J. Appl. Phys. **109**(8), 084110 (2011).
71. G. Liu, H. Zhao, J. Zhang, J. H. Park, L. J. Mawst, and N. Tansu, "Selective area epitaxy of ultra-high density InGaN quantum dots by diblock copolymer," Nanoscale Res. Lett. **6**(1), 342 (2011).
72. Y. R. Wu, Y. Y. Lin, H. H. Huang, and J. Singh, "Electronic and optical properties of InGaN quantum dot based light emitters for solid state lighting," J. Appl. Phys. **105**(1), 013117 (2009).
73. J. Zhang, H. Zhao, and N. Tansu, "Effect of crystal-field split-off hole and heavy-hole bands crossover on gain characteristics of high Al-content AlGaN quantum well lasers," Appl. Phys. Lett. **97**(11), 111105 (2010).
74. T. Kolbe, A. Knauer, C. Chua, Z. Yang, S. Einfeldt, P. Vogt, N. M. Johnson, M. Weyers, and M. Kneissl, "Optical polarization characteristics of ultraviolet (In)(Al)GaN multiple quantum well light emitting diodes," Appl. Phys. Lett. **97**(17), 171105 (2010).
75. T. K. Sharma and E. Towe, "Impact of strain on deep ultraviolet nitride laser and light-emitting diodes," J. Appl. Phys. **109**(8), 086104 (2011).
76. J. Zhang, H. Zhao, and N. Tansu, "Large optical gain AlGaN-Delta-GaN quantum wells laser active regions in mid- and deep-ultraviolet spectral regimes," Appl. Phys. Lett. **98**(17), 171111 (2011).
77. M. Krames, O. Shchekin, R. Mueller-Mach, G. Mueller, L. Zhou, G. Harbers, and M. Craford, "Status and future of high-power light-emitting diodes for solid-state lighting," J. Disp. Technol. **3**(2), 160–175 (2007).
78. M. H. Kim, M. F. Schubert, Q. Dai, J. K. Kim, E. F. Schubert, J. Piprek, and Y. Park, "Origin of efficiency droop in GaN-based light-emitting diodes," Appl. Phys. Lett. **91**(18), 183507 (2007).
79. M. F. Schubert, J. Xu, J. K. Kim, E. F. Schubert, M. H. Kim, S. Yoon, S. M. Lee, C. Sone, T. Sakong, and Y. Park, "Polarization-matched GaInN/AlGaInN Multi-quantum-well light-emitting diodes with reduced efficiency droop," Appl. Phys. Lett. **93**(4), 041102 (2008).
80. Y. C. Shen, G. O. Mueller, S. Watanabe, N. F. Gardner, A. Munkholm, and M. R. Krames, "Auger recombination in InGaN measured by photoluminescence," Appl. Phys. Lett. **91**(14), 141101 (2007).
81. K. T. Delaney, P. Rinke, and C. G. Van de Walle, "Auger recombination rates in nitrides from first principles," Appl. Phys. Lett. **94**(19), 191109 (2009).
82. E. Kioupakis, P. Rinke, K. T. Delaney, and C. G. Van de Walle, "Indirect Auger recombination as a cause of efficiency droop in nitride light-emitting diodes," Appl. Phys. Lett. **98**(16), 161107 (2011).
83. S. F. Chichibu, T. Azuhata, M. Sugiyama, T. Kitamura, Y. Ishida, H. Okumura, H. Nakanishi, T. Sota, and T. Mukai, "Optical and structural studies in InGaN quantum well structure laser diodes," J. Vac. Sci. Technol. B **19**(6), 2177 (2001).
84. J. Xie, X. Ni, Q. Fan, R. Shimada, U. Ozgur, and H. Morkoc, "On the efficiency droop in InGaN multiple quantum well blue light emitting diodes and its reduction with p-doped quantum well barriers," Appl. Phys. Lett. **93**(12), 121107 (2008).
85. X. Ni, Q. Fan, R. Shimada, U. Ozgur, and H. Morkoc, "Reduction of efficiency droop in InGaN light emitting diodes by coupled quantum wells," Appl. Phys. Lett. **93**(17), 171113 (2008).
86. A. A. Efremov, N. I. Bochkareva, R. I. Gorbunov, D. A. Lavrinovich, Y. T. Rebane, D. V. Tarkhin, and Y. G. Shreter, "Effect of the Joule heating on the quantum efficiency and choice of thermal conditions for high-power blue InGaN/GaN LEDs," Semiconductors **40**(5), 605–610 (2006).
87. J. Hader, J. V. Moloney, B. Pasenow, S. W. Koch, M. Sabathil, N. Linder, and S. Lutgen, "On the importance of radiative and Auger losses in GaN-based quantum wells," Appl. Phys. Lett. **92**(26), 261103 (2008).
88. W. W. Chow, M. H. Crawford, J. Y. Tsao, and M. Kneissl, "Internal efficiency of InGaN light-emitting diodes: beyond a quasiequilibrium model," Appl. Phys. Lett. **97**(12), 121105 (2010).
89. N. F. Gardner, G. O. Muller, Y. C. Shen, G. Chen, S. Watanabe, W. Gotz, and M. R. Krames, "Blue-emitting InGaN-GaN double-heterostructure light-emitting diodes reaching maximum quantum efficiency above 200 A/cm^2," Appl. Phys. Lett. **91**(24), 243506 (2007).
90. H. Zhao, G. Liu, R. A. Arif, and N. Tansu, "Current injection efficiency induced efficiency-droop in InGaN quantum well light-emitting diodes," Solid-State Electron. **54**(10), 1119–1124 (2010).
91. S. Choi, H. J. Kim, S.-S. Kim, J. Liu, J. Kim, J.-H. Ryou, R. D. Dupuis, A. M. Fischer, and F. A. Ponce, "Improvement of peak quantum efficiency and efficiency droop in iii-nitride visible light-emitting diodes with an InAlN electron-blocking layer," Appl. Phys. Lett. **96**(22), 221105 (2010).
92. H. J. Kim, S. Choi, S.-S. Kim, J.-H. Ryou, P. D. Yoder, R. D. Dupuis, A. M. Fischer, K. W. Sun, and F. A. Ponce, "Improvement of quantum efficiency by employing active-layer-friendly lattice-matched InAlN electron blocking layer in green light-emitting diodes," Appl. Phys. Lett. **96**(10), 101102 (2010).

1. Introduction

III-Nitride semiconductors have significant applications for solid state lighting and lasers [1–20], power electronics [21], thermoelectricity [22,23], and solar cells [24–26]. The InGaN quantum wells (QWs) employed as active region for nitride light-emitting diodes (LEDs) covers the wide spectral regime from near ultraviolet to near infrared [1–20]. As the emission wavelength of the InGaN QWs extends from blue to green and red spectral regimes, the

#147902 - $15.00 USD Received 19 May 2011; accepted 22 Jun 2011; published 1 Jul 2011
(C) 2011 OSA

internal quantum efficiency (IQE) in InGaN QWs LEDs decreases significantly due to (1) high dislocation density results from the lattice mismatch between the sapphire substrate and GaN / InGaN leading to large non-radiative recombination rate, and (2) charge separation from the polarization fields in the QW leading to reduction of the electron-hole wavefunction overlap (Γ_{e_hh}) and radiative recombination rate (R_{sp}) in particular for green-emitting QWs. Recent works have reported the growths of highly-abrupt interfaces between InGaN QWs and GaN barriers with no indium clustering [27]. In addition, the existence of spontaneous and piezoelectric polarization fields in InGaN QWs [28–34] led to charge separation effect, which in turn impacts both the radiative recombination rate and carrier dynamics in the QWs [35–37]. In order to maximize the external quantum efficiency of nitride LEDs, the optimizations of both extraction efficiency and IQE of the LEDs are of great importance. Various methods have been pursued to optimize the light extraction efficiency in nitride LEDs [15–20].

It is important to note that the reduction in dislocation densities in nitride alloy is also instrumental in reducing the non-radiative recombination rate in the LEDs, which will also lead to enhancement in the radiative efficiency of the devices [38–42]. Recently, the elimination of V-defect in InGaN QWs had been reported resulting in enhancement in the IQE of the LEDs [38,39]. Recent works had reported a threading dislocation density reduction in blue- and green-emitting InGaN LEDs grown on nanopatterned sapphire substrates [41,42].

Recently, several approaches have been proposed to suppress the charge separation issue by employing novel QWs with improved electron-hole wavefunction overlap (Γ_{e_hh}) such as (1) nonpolar InGaN QWs [43–45], (2) staggered InGaN QW [46–58], (3) InGaN QW with δ-AlGaN layer [59,60], (4) type-II InGaN QW [61–63], (5) InGaN-delta-InN QW [64], and (6) triangular QWs [65]. These approaches used various methods to engineer the InGaN QWs in order to obtain structures with large optical matrix elements, which in turn lead to significantly improved radiative recombination rate. Other approach based on strain compensated InGaN QW design [66] had also been proposed to enhance the IQE of the LED, and recent experimental works [67] showed good agreement with theory. Recently, the use of staggered QWs [46–58] had also been implemented in ZnO / ZnMgO QWs structures [68].

In this paper, we investigated the approaches based on quantum well structures with large overlap design to enhance the internal quantum efficiency (IQE) for InGaN QWs based LEDs. The optimization of both radiative efficiency and current injection efficiency for InGaN QWs is crucial for the enhancement of the IQE of the QWs. Staggered InGaN QWs are analyzed as active region for nitride LEDs with enhanced electron-hole wavefunction overlap (Γ_{e_hh}). The effect of abruptness of interface in staggered InGaN QWs on Γ_{e_hh} and radiative recombination rate (R_{sp}) is studied. In addition, the effect of current injection efficiency on efficiency droop in InGaN QWs is studied. Novel structures designed by employing thin large band gap barrier materials surrounding the InGaN QWs to suppress the efficiency droop are discussed. The optimization of both radiative efficiency and current injection efficiency in InGaN QWs enables the realization of high internal quantum efficiency for nitride based LEDs emitting in the green wavelength region and longer.

The organization of this paper is presented as follows. Section 2 introduces the concept of band structure engineering for InGaN QWs with large electron-hole wavefunction overlap / large momentum matrix element. In Section 3, the staggered InGaN QWs for high internal quantum efficiency green LEDs are presented. The effect of abruptness of interface in staggered InGaN QWs is discussed in Section 4. Section 5 presents the epitaxy and characteristics of linearly-shaped staggered InGaN QWs. Section 6 discusses the issues and approaches to address the efficiency droop in InGaN QWs LEDs, as well as other important issues related to the internal quantum efficiency enhancement in InGaN QWs LEDs.

2. Band engineering of InGaN QWs for large electron-hole wavefunction overlap

In conventional c-plane InGaN QWs, the existence of strong electrostatic fields leads to strong energy band bending for both conduction band and valence band in the QW [28–34], which result in the spatial separation of the electrons and holes and reduce the electron-hole

#147902 - $15.00 USD Received 19 May 2011; accepted 22 Jun 2011; published 1 Jul 2011
(C) 2011 OSA

wavefunction overlap (Γ_{e_hh}) [35–37]. The charge separation issue becomes more severe for InGaN QWs with emission wavelength extended in the green and longer spectral regimes.

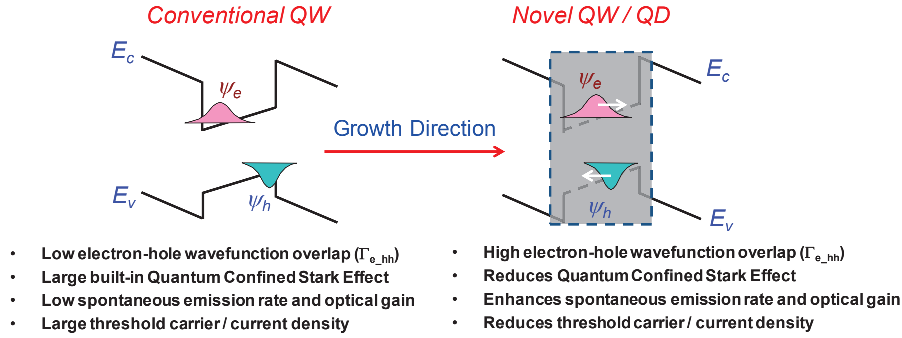

Fig. 1. The concept of novel InGaN QWs / QDs structures with improved electron-hole wavefunction overlap.

To resolve the fundamental issue for the conventional InGaN QW based LEDs due to the low electron-hole wavefunction overlap (Γ_{e_hh}), novel QW structures with enhanced overlap Γ_{e_hh} are important to achieve active regions with large spontaneous emission radiative recombination rate (R_{sp}) [43–65]. As illustrated in Fig. 1, by employing novel QW designs, the shift of the electron and hole wavefunctions toward the center of the QW leads to the reduction of the charge separation and enhancement of the electron-hole wavefunction overlap (Γ_{e_hh}). Based on the Fermi's golden rule, the transition matrix element is proportional to the square of the electron-hole wavefunction overlap ($|\Gamma_{e_hh}|^2$) [46]. Thus, with the enhanced Γ_{e_hh}, the spontaneous emission radiative recombination rate will be enhanced. The improved optical matrix element leads to high R_{sp}, which in turn enables the realization of high brightness nitride LEDs emitting in green spectral regime or beyond.

3. Staggered InGaN QWs for high internal quantum efficiency green LEDs

The purpose of using the staggered InGaN QW design is to enhance the electron-hole wavefunction overlap (Γ_{e_hh}) by engineering the band lineups of the InGaN QW, hence leading to an increase in the radiative recombination rate (R_{sp}) of the QW for LEDs application. The concept of staggered InGaN QW has been introduced in references 46–58, which can be implemented as active regions in typical nitride-based LED devices [15–20].

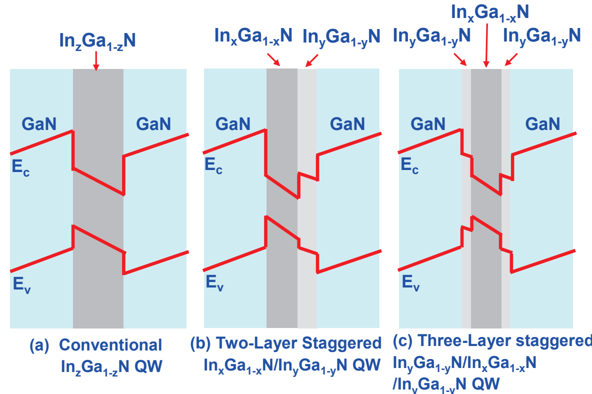

Fig. 2. Schematics of the (a) conventional $In_zGa_{1-z}N$-GaN QW; (b) two-layer staggered $In_xGa_{1-x}N$ / $In_yGa_{1-y}N$ QW; and (c) three-layer staggered $In_yGa_{1-y}N$ / $In_xGa_{1-x}N$ / $In_yGa_{1-y}N$ QW structures [47].

#147902 - $15.00 USD
Received 19 May 2011; accepted 22 Jun 2011; published 1 Jul 2011
(C) 2011 OSA

Figure 2 shows the schematics of (a) a conventional $In_zGa_{1-z}N$ QW; (b) a two-layer staggered $In_xGa_{1-x}N$ / $In_yGa_{1-y}N$ QW and (c) a three-layer staggered $In_yGa_{1-y}N$ / $In_xGa_{1-x}N$ / $In_yGa_{1-y}N$ QW structures, which are surrounded by the GaN barriers [47]. Note that the three structures were designed with identical total QW thickness (d_{QW}) for comparison purpose. The studies of the characteristics of these staggered InGaN QW LEDs were presented in references 47 and 48, and the analysis indicated that the use of green-emitting staggered InGaN QW active region leads to significant enhancement in the radiative recombination rate by ~5-6 times for the optimized three-layer staggered InGaN QW structure [47]. These results in turn correspond to ~1.5-2.5 times enhancement in the expected increase in the radiative efficiency of the InGaN QWs LEDs [47].

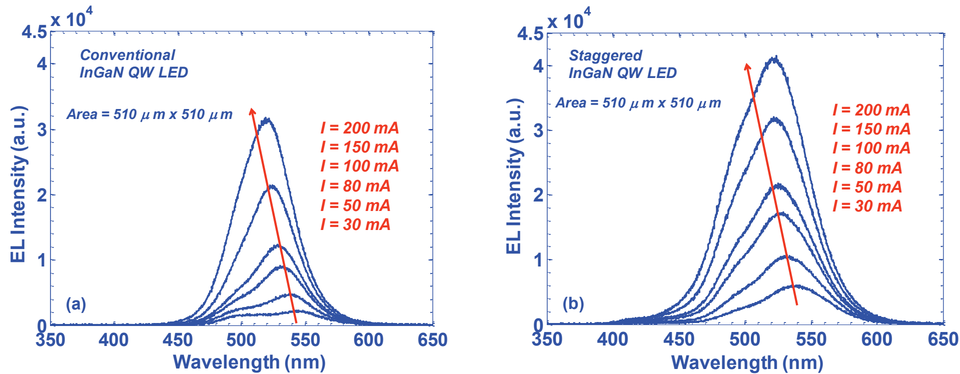

Fig. 3. The electroluminescence spectra for (a) conventional InGaN QW and (b) three-layer staggered InGaN QW LEDs emitting with peak wavelengths at 520-525 nm, as function of injection current levels.

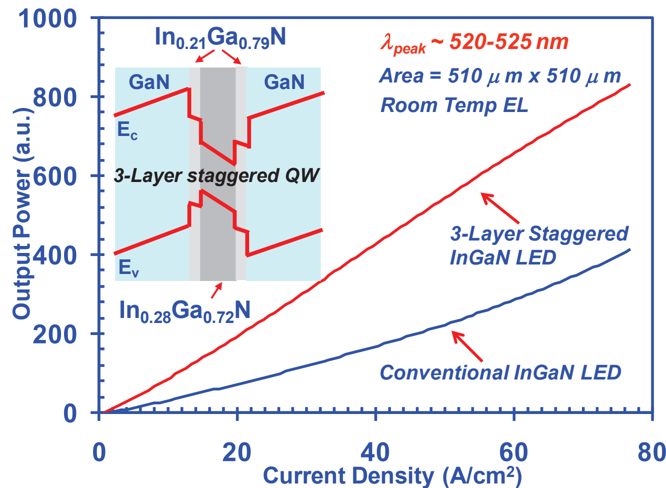

Fig. 4. Light output power vs current density for conventional InGaN QW and three-layer staggered InGaN QW LEDs at λ~520–525 nm, with the band lineups schematic of three-layer staggered InGaN QW [48].

In order to carry out the experimental studies of the three-layer staggered InGaN QW LEDs, the use of graded growth temperature technique in metalorganic chemical vapor deposition (MOCVD) was employed for the epitaxy of the active region [48]. The detail of the growth method was presented in reference 48. Figures 3(a) and 3(b) show the electrical luminescence (EL) for the conventional InGaN QWs LED and three-layer staggered InGaN QWs LED emitting at 520-525 nm, measured under continuous wave (CW) operation at room

#147902 - $15.00 USD Received 19 May 2011; accepted 22 Jun 2011; published 1 Jul 2011
(C) 2011 OSA

temperature [48]. Both devices were based on bottom-emitting square device, with area size of 510 µm x 510 µm. The enhancement of the peak EL for the three-layer staggered InGaN LED as compared to the conventional LED is 1.8 times (1.3 times) at I = 100 mA (I = 200 mA). The FWHMs of the EL spectra for the three-layer staggered InGaN QW LEDs were measured as larger [Fig. 3(b)], in comparison to those of the conventional LEDs. The larger FWHMs of the EL spectra were more obvious for increasing current density, which can be attributed to the less abrupt interfaces in the three-layer staggered InGaN QW active region. The output powers versus the inject current density for conventional and three-layer staggered InGaN LEDs measured under continuous wave operation were shown in Fig. 4. The output power of the three-layer staggered InGaN QW LED was measured as ~2.0 times higher in comparison to that measured from conventional LEDs at high current density. The findings obtained from experiments are in good agreement with that predicted from theory.

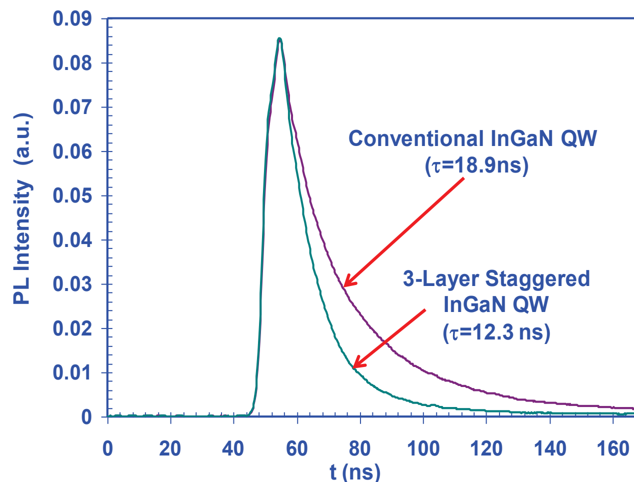

Fig. 5. Time resolved measurements on both 3-layer staggered InGaN QW and conventional InGaN QW LED samples, with peak emission wavelength at 520-525 nm. The measurements were carried out by employing 430-nm excitation lasers with pulse duration of 25 ps [48].

In order to obtain the understanding of the carrier dynamic and recombination from the staggered InGaN QW LEDs, the time resolved photoluminescence (TR-PL) measurements were performed for both conventional and three-layer staggered InGaN QW LED samples emitting at 520-525 nm [48]. The TR-PL measurements were carried out by utilizing a Nd:YAG laser that is doubled and tripled in frequency and whose ultraviolet output pumps an optical parametric generator / amplifier system that ultimately delivers short optical pulses with a wavelength than can be tuned from 420 nm up to 2 µm in the infrared. The excitation laser wavelength of 430-nm was employed for the measurements of the InGaN QWs samples. The pulse duration, repetition rate, output power and beam diameter for the excitation laser were 25 ps, 10 Hz, 30 µJ / pulse, and ~300 µm, respectively. The emission from the InGaN QW LEDs was detected by a photomultiplier tube (Thermo Oriel Instruments 70705). The time evolution of photoluminescence from the InGaN QWs was collected and displayed by the Lecroy LT584 oscilloscope (1 GHz bandwidth). As shown in Fig. 5, the TR-PL measurements for both staggered ($\tau_{staggered}$ = 12.3 ns) and conventional ($\tau_{conventional}$ = 18.9 ns) InGaN LEDs indicated a 35% reduction of carrier lifetime for the staggered In aN QW LEDs. The TR-PL measurements for PL samples (with no p-GaN cap layer) show the similar reduction of the carrier lifetime for the staggered InGaN QWs. As compared with the conventional InGaN QW LEDs, the staggered InGaN QW LEDs show enhanced radiative efficiency, output power, and reduced carrier lifetime, which indicated that the increase in radiative recombination rate from the enhanced electron-hole wavefunction overlap is a dominant factor for the improved device performance.

#147902 - $15.00 USD Received 19 May 2011; accepted 22 Jun 2011; published 1 Jul 2011
(C) 2011 OSA

Based on the following parameters, the carrier density in the InGaN QW active region during the carrier lifetime measurement is estimated: (1) the 430-nm excitation laser power (30 μJ / pulse), (2) the laser beam diameter (~300 μm), (3) the absorption coefficient for InGaN material (α_{QW} ~2 x 10^3 cm^{-1}) [69], and (4) the total thickness of the InGaN 4-QWs active region of 12 nm. Thus, the estimated carrier density in the InGaN QW is in the range of mid-10^{19} cm^{-3}. In order to estimate the monomolecular recombination coefficient (A) and Auger recombination coefficient (C) for the conventional and staggered InGaN QWs, the total carrier lifetimes are calculated for both conventional InGaN QW and three-layer staggered InGaN QW emitting at ~525 nm at different carrier density as shown in Fig. 6. Based on the carrier lifetime measurements for both conventional ($\tau_{conventional}$ = 18.9 ns) and staggered ($\tau_{staggered}$ = 12.3 ns) InGaN QWs, the estimated carrier density in InGaN QW active region is about n ~5x10^{19} cm^{-3}. In our analysis, we have made the assumption that the monomolecular coefficient (A) and Auger coefficient (C) for both conventional and staggered InGaN QWs as identical. From Fig. 6, the estimated monomolecular recombination coefficient (A) and Auger coefficient (C) that match with the experimental measurements are A ~1.6x10^7 s^{-1} and C~5x10^{-33} cm^6s^{-1}. Based on the estimated monomolecular coefficient and Auger coefficient, the radiative carrier lifetimes (τ_{rad}) for both three-layer staggered InGaN QWs and conventional InGaN QWs emitting at λ ~520-525 nm can be estimated as ~18.58 ns and ~39.35 ns, respectively, for carrier density n ~5x10^{19} cm^{-3}. The finding indicates that the use of three-layer staggered InGaN QWs leads to ~2.12 times increase in radiative recombination rate, in comparison to that measured for conventional InGaN QWs.

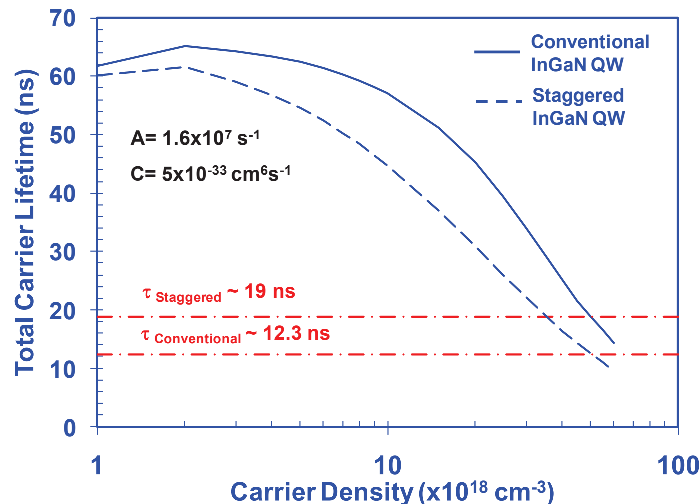

Fig. 6. Total carrier lifetime as a function of carrier density for conventional InGaN QW and staggered InGaN QW at monomolecular coefficient A = 1.6x10^7 s^{-1} and Auger coefficient C = 5x10^{-33} cm^6s^{-1}.

Note that the approaches of suppressing charge separation effect in InGaN QWs discussed here are also applicable for InGaN quantum dots (QDs) active regions [70–72]. Several approaches by engineering the InGaN QDs have been pursued in order to achieve higher spontaneous emission rate by achieving structures with larger optical matrix elements [70–72]. In contrast to InGaN QWs, one of key limitations for AlGaN-based deep- and mid-UV LEDs and lasers is related to the valence band arrangement of heavy-hole (HH) and crystal-field split-off hole (CH) bands [73–75]. Thus, the optimization for AlGaN QWs requires other method focusing on the use of novel QW structures that allow valence band lineups engineering in the active region [76].

4. Effect of abruptness of interface for staggered InGaN QWs

In this section, the effect of interface linear grading on the electron-hole wavefunction overlap and spontaneous emission radiative recombination rate will be analyzed for the staggered InGaN QWs. Here we assume that the interface between the staggered InGaN QWs sub-layers contains the transition InGaN layer with linearly-graded In-content profile. Five staggered InGaN QWs structures with various thicknesses of transition InGaN layers (2-Å, 4-Å, 6-Å, 8-Å and 10-Å interface In-content linear-grading) are compared with the staggered InGaN QWs with abrupt In-content interface (0-Å interface In-content linear-grading). Figure 7 shows the energy band lineups and the corresponding electron and hole wavefunctions for the staggered 6-Å $In_{0.14}Ga_{0.86}N$ / 18-Å $In_{0.3}Ga_{0.7}N$ / 6-Å $In_{0.14}Ga_{0.86}N$ QWs with: (a) 0-Å interface In-content linear-grading, and (b) 6-Å interface In-content linear-grading.

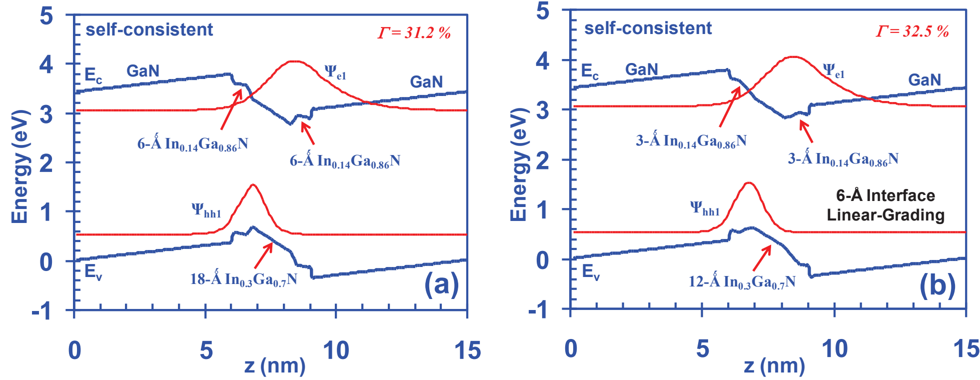

Fig. 7. Energy band lineups and electron, hole wavefunction for staggered InGaN QWs with (a) 0-Å interface In-content linear-grading; (b) 6-Å interface In-content linear-grading.

From Fig. 7, we observed that the band lineups for the staggered InGaN QWs with a linear gradient of the In-content linear-grading [Fig. 7(b)] are significantly-less abrupt as compared to those for the staggered InGaN QWs with abrupt In-content interface [Fig. 7(a)]. However, both electron and hole wavefunctions exhibited relatively similar distribution for both staggered InGaN QWs with abrupt and less abrupt interfaces. Thus, the electron-hole wavefunction overlap (Γ_{e_hh}) for the staggered InGaN QWs shown in Fig. 7(b) have relatively minor modification.

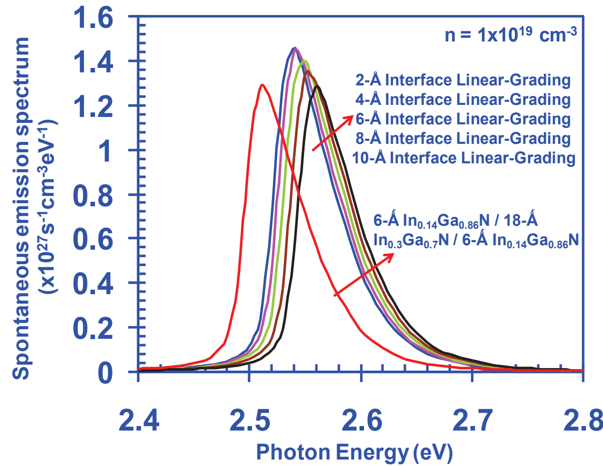

Fig. 8. R_{sp} spectra for staggered InGaN QWs with less abrupt interface by In-content linear-grading.

#147902 - $15.00 USD Received 19 May 2011; accepted 22 Jun 2011; published 1 Jul 2011
(C) 2011 OSA

To investigate the effect of the In-content linear-grading on the spontaneous emission radiative recombination rate (R_{sp}), the calculations of R_{sp} were performed for the six staggered InGaN QWs structures as discussed. The comparison of the R_{sp} spectra calculated at the carrier density of n = $1x10^{19}$ cm^{-3} for staggered InGaN QWs is shown in Fig. 8. From Fig. 8, we observe slight modification on the R_{sp} spectra including slight modification on the spontaneous emission peak intensity and integrated intensity. Slight blue shifts in the peak wavelength are also observed for the staggered InGaN QWs with less abrupt interfaces. Thus, the In-content with linear-grading between the InGaN sub-layers in the staggered InGaN QWs will not lead to the degradation of the QW performance. The graded growth temperature technique introduced for the metalorganic chemical vapor deposition (MOCVD) of the staggered InGaN QWs [48,49] is expected to introduce less-abrupt interface in the sub layers of the QWs. However, our finding shows that the introduction of less-abrupt interface does not lead to any reduction in spontaneous emission rate in the QW, which shows that the use of graded growth temperature approach is practical for manufacturing of staggered QW LEDs.

5. Linearly-shaped staggered InGaN QWs

5.1 MOCVD of linearly-shaped (LS) staggered InGaN QWs

Similar to the concept of three-layer staggered InGaN QW, QWs designed with local minima in the center will result in the shift of both electron and hole wavefunction toward the center of the QW region, which leads to significant enhancement in the electron-hole wavefunction overlap (Γ_{e_hh}) and spontaneous emission rate.

By controlling the growth temperature during the InGaN QW layers epitaxy, various In-content can be obtained in the InGaN QWs. By using the current control mode to control the growth temperature during the staggered InGaN QWs growths, the real growth temperature profile for the staggered InGaN QWs shows stable temperature control as well as fast temperature modification. The ability to achieve very precise good control of the growth temperature by using the current control mode led to the ability to achieve higher degree of control in the Indium contents in the sub-layers of the staggered InGaN QWs.

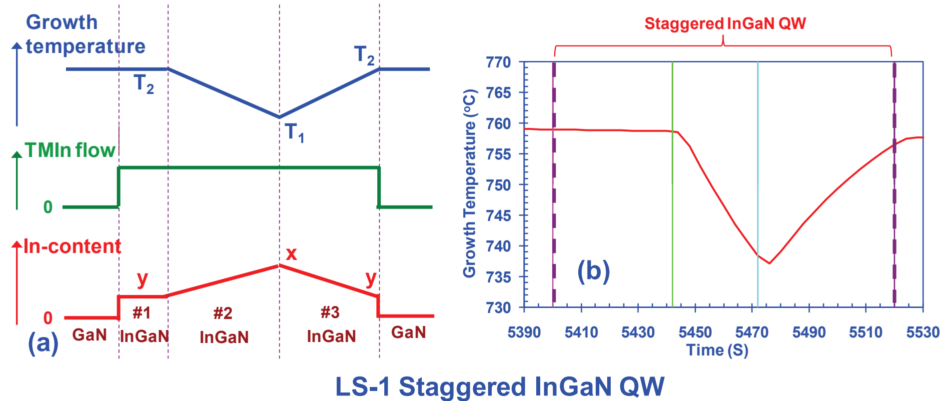

Fig. 9. Schematics of the growth temperature, TMIn-flow rate, and In-content for the LS-1 staggered InGaN QW [Fig. 9(a)] and the corresponding real growth temperature profiles [Fig. 9(b)].

Figures 9–11 show the schematics of three different linearly-shaped (LS) staggered InGaN QWs [LS-1 staggered QW (Fig. 9), LS-2 staggered QW (Fig. 10) and LS-3 staggered QW (Fig. 11)]. The left figures [Figs. 9(a), 10(a) and 11(a)] correspond to the schematics of the designed growth temperature profiles and the In-content profiles. Note that the TMIn flow was kept constant for all the experiments. The bottom figures [Figs. 9(b), 10(b) and 11(b)] show the real growth temperature profiles by MOCVD using the current control mode. By comparing Figs. 9(a), 10(a), 11(a) with Figs. 9(b), 10(b) and 11(b), the real growth

#147902 - $15.00 USD Received 19 May 2011; accepted 22 Jun 2011; published 1 Jul 2011
(C) 2011 OSA

temperature profiles match very well with the schematics. In contrast to the LS staggered InGaN QW, the conventional InGaN QWs contain constant In-content for the InGaN QW, where the growth temperature for the conventional InGaN QW is constant.

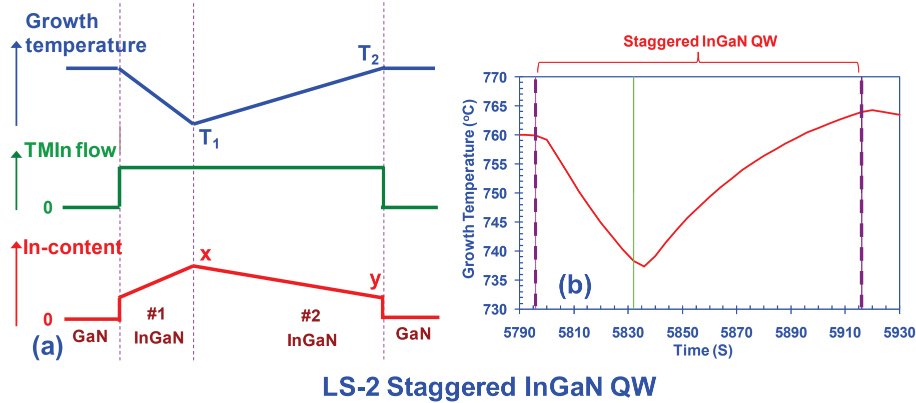

Fig. 10. Schematics of the growth temperature, TMIn-flow rate, and In-content for the LS-2 staggered InGaN QW [Fig. 10(a)] and the corresponding real growth temperature profiles [Fig. 10(b)].

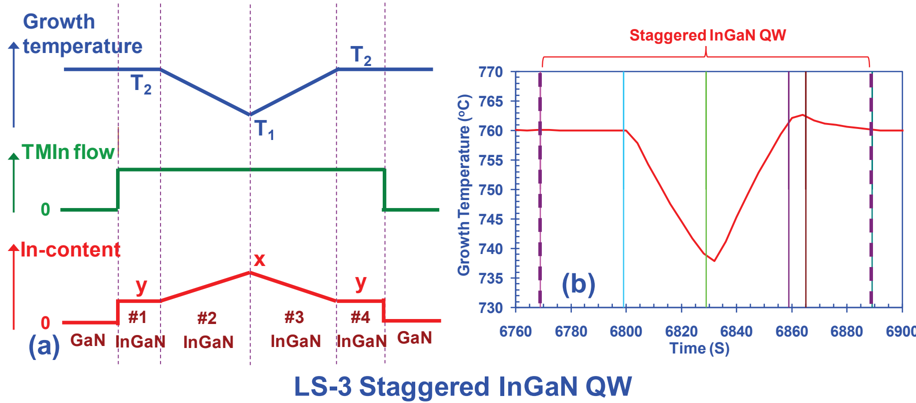

Fig. 11. Schematics of the growth temperature, TMIn-flow rate, and In-content for the LS-3 staggered InGaN QW [Fig. 11(a)] and the corresponding real growth temperature profiles [Fig. 11(b)].

During the MOCVD growth, TMGa / TEGa, TMIn, and NH_3 were used as gallium, indium, and nitrogen precursors, respectively. Cp_2Mg and dilute SiH_4 were used as p- and n-type dopant sources, respectively. The growth of InGaN active layer employs TMIn, TEGa and NH_3 as the precursors, and N_2 gas was employed as carrier gas. The V/III and [TMIn] / [III] molar ratios for the growth of InGaN layers were kept constant at 20700 and 0.56, respectively. Both conventional and LS staggered InGaN QW LEDs emitting at 460-480 nm were grown on 2.5 µm thick n-doped GaN (n = $4x10^{18}$ cm^{-3}) on c-plane double-side polished sapphire substrate, employing a low temperature 30-nm GaN buffer layer. Both conventional and linearly-shaped staggered InGaN QW structures consist of 4-period of InGaN QWs with 10 nm undoped GaN barriers. The conventional InGaN QW was grown at 750 °C, and the LS staggered InGaN QWs were grown at varied temperature profiles as shown in Figs. 9(b), 10(b) and 11(b) ranging between 738 °C and 760 °C. The thickness of the LS staggered InGaN QW is calibrated as 3 nm, which is similar to that of conventional InGaN QW. On top of the InGaN QWs, 200 nm p-GaN (p = $3x10^{17}$ cm^{-3}) were employed as p-type layer.

#147902 - $15.00 USD Received 19 May 2011; accepted 22 Jun 2011; published 1 Jul 2011
(C) 2011 OSA

5.2 Cathodoluminescence measurement of linearly-shaped staggered InGaN QWs

The luminescence characteristics of both conventional and linearly-shaped staggered InGaN QWs samples were studied by power-density-dependent cathodoluminescence (CL) measurements performed at T = 300K. We utilized a 10 keV electron beam in spot mode (area = 2.0 x 10^{-9} cm^2) to excite the InGaN QWs active region. To study the effect of the excitation power on the CL intensity for both conventional and linearly-shaped staggered InGaN QW LEDs, different excitation power density levels were applied on both conventional and linearly-shaped staggered InGaN QW LED samples. The various excitation power densities for a constant volume were obtained by varying the electron beam current (with constant accelerating voltage of 10 keV) from 20 nA up to 800 nA.

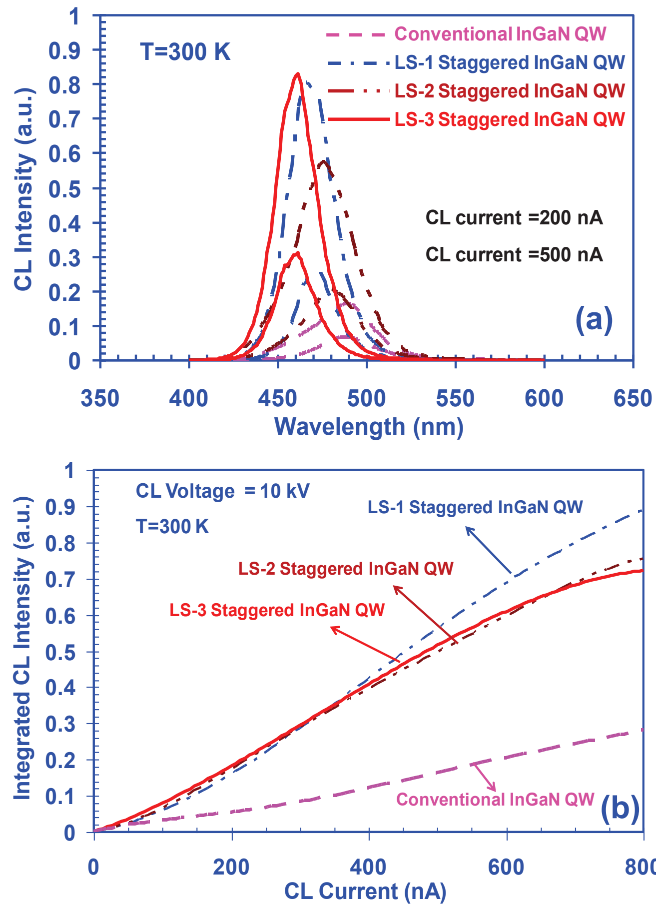

Fig. 12. (a) CL spectra of conventional, LS-1 staggered, LS-2 staggered, and LS-3 staggered InGaN QWs emitting at 460-480nm with various CL excitation currents; (b) Integrated CL intensity of conventional, LS-1 staggered, LS-2 staggered, and LS-3 staggered InGaN QW versus CL excitation currents at T = 300K.

Figure 12(a) shows the measured CL spectra plotted against CL pump current (shown for 200 nA and 500 nA) of the conventional, LS-1 staggered InGaN QW, LS-2 staggered InGaN QW, and LS-3 staggered InGaN QW. The linearly-shaped staggered InGaN QW samples exhibit improved peak luminescence by 2.8-5.1 times of that of the conventional InGaN QW. Note that the linearly-shaped staggered InGaN QWs show slight blue shift as compared to the conventional InGaN QW due to the ramping up of the growth temperature during the growths of QWs, which requires further optimization of the growth temperature profile to match the emission wavelength to that of the conventional InGaN QWs. Integrated CL intensities for

#147902 - $15.00 USD Received 19 May 2011; accepted 22 Jun 2011; published 1 Jul 2011
(C) 2011 OSA

both QWs LEDs were obtained by integration of the CL spectra data over the photon energy [Fig. 12(b)]. The LS-1 (LS-2, and LS-3) staggered InGaN QW exhibited improvement by 1.35-3.2 (1.8-2.7, and 2.1-2.6) times of the integrated CL intensity as compared to that of the conventional QW. Both conventional and LS staggered InGaN QWs LEDs show blue-shift in emission wavelengths as the pumping current increases due to the carrier screening effect.

5.3 Numerical Simulation of Linearly-Shaped Staggered InGaN QWs

To numerically study the effect of the linearly-shaped staggered InGaN QWs on the spontaneous emission radiative recombination (R_{sp}), the R_{sp} properties of LS-3 staggered InGaN QW is calculated and compared to that of the conventional InGaN QW. Figure 13 shows the band lineups for (a) conventional 30-Å $In_{0.25}Ga_{0.75}N$ QW and (b) LS-3 staggered InGaN QW, with the design wavelength at λ~500 nm. The detailed structure for LS-3 staggered InGaN QW is shown in Fig. 13(c), which comprises two side layers of 5-Å $In_{0.18}Ga_{0.82}N$ layers and linearly-shaped $In_xGa_{1-x}N$ layers (0.18<x<0.4). From Figs. 13(a) and 13(b), the electron-hole wavefunction overlap (Γ_{e_hh}) is significantly enhanced from 17.3% (conventional InGaN QW) to 32.8% by utilizing the LS-3 staggered InGaN QW. The enhancement of the Γ_{e_hh} is due to the shift of both electron and hole wavefunctions toward the center of the QW region from the band lineups engineering. The use of LS staggered InGaN QWs can be practically implemented by using graded growth temperature approach.

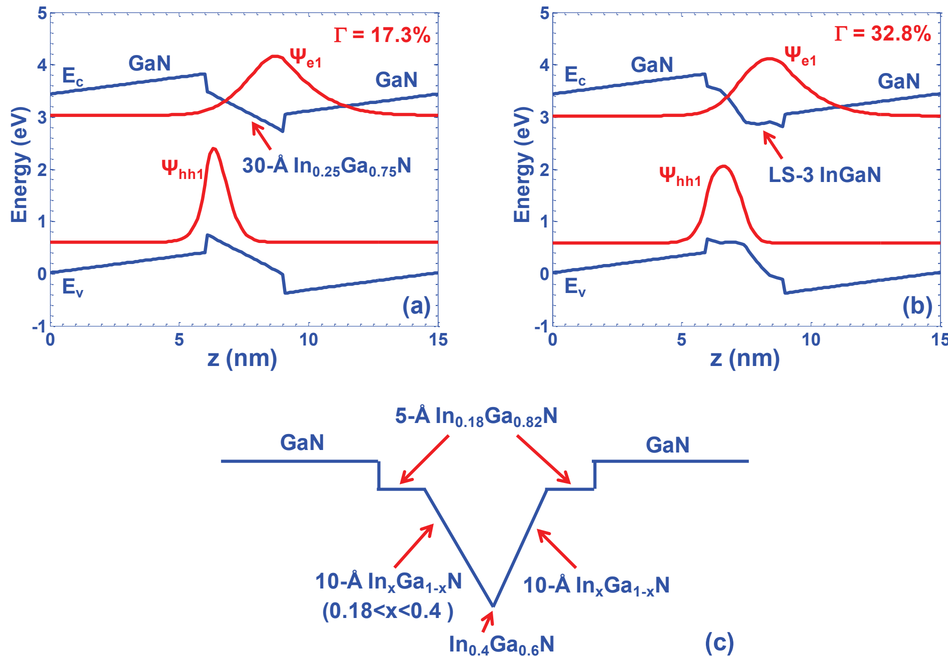

Fig. 13. Band lineups and electron and hole wavefunction for (a) conventional 30-Å InGaN QWs and (b) LS-3 staggered InGaN QW. (c) Schematic of the conduction band lineup without the polarization field for LS-3 staggered InGaN QW with GaN barriers, where the sub-layers at side contain 5-Å $In_{0.18}Ga_{0.82}N$, and the linearly-shaped 10-Å $In_xGa_{1-x}N$ contain InGaN layers with In-content linearly modified from 0.18 to 0.4.

The spontaneous emission spectra are calculated for both conventional InGaN QW and LS-3 staggered InGaN QW. Figure 14(a) shows the spontaneous emission spectra for both two structures at carrier density from n = $1x10^{18}$ cm^{-3} up to n = $2x10^{19}$ cm^{-3}. Both structures are designed emitting at the similar wavelength (~500 nm). From Fig. 14(a), we observe significant enhancement in the spontaneous emission at different carrier density. In addition, the LS-3 staggered InGaN QW shows less blue-shift of the peak emission wavelength as the

#147902 - $15.00 USD
Received 19 May 2011; accepted 22 Jun 2011; published 1 Jul 2011
(C) 2011 OSA

carrier density increases as compared to that of the conventional InGaN QW. Figure 14(b) shows the comparison of the spontaneous emission rate (R_{sp}) for both conventional and LS-3 staggered InGaN QWs. The R_{sp} is obtained by integrating the spontaneous emission spectrum over the photon energy. The R_{sp} for the LS-3 staggered InGaN QW shows 3.2-3.9 times enhancement as compared to that of the conventional InGaN QW at different carrier density.

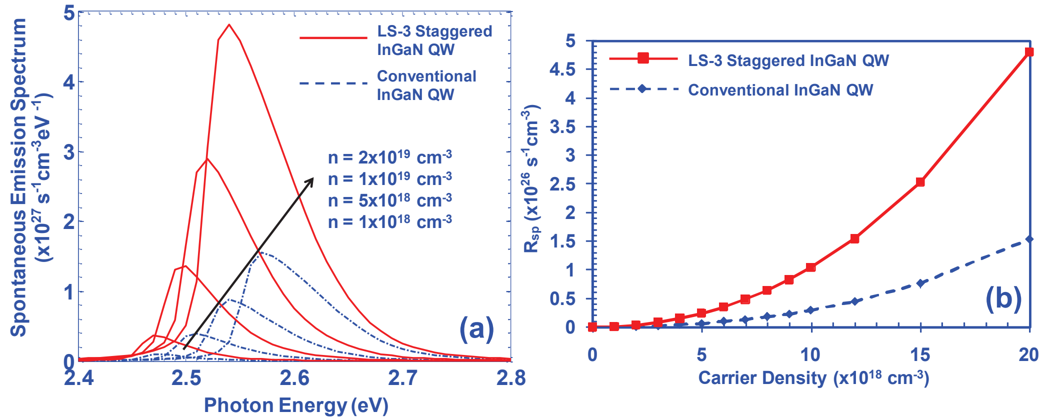

Fig. 14. (a) Spontaneous emission spectra for conventional InGaN QW and LS-3 staggered InGaN QW with carrier density from $1x10^{18}$ cm^{-3} up to $2x10^{19}$ cm^{-3}; (b) spontaneous emission radiative recombination rate (R_{sp}) for conventional InGaN QW and LS-3 staggered InGaN QW at different carrier density upto $2x10^{19}cm^{-3}$.

6. Other issues for IQE in InGaN QW LEDs—defects and efficiency droop

In addition to the approaches to address the charge separation in InGaN QWs, the reduction of threading dislocation and V-defects in InGaN QW is also of great importance for ensuring high radiative efficiency and IQE of the devices [38–42]. Recent works by growing on nanopatterned sapphire substrates have resulted in threading dislocation density reduction [41,42]. The uses of low-dislocation substrates and novel growth methods have resulted in reduction in V-defects in InGaN QWs [38–40]. In addition to the optimization of the radiative efficiency ($\eta_{Radiative}$) by increasing the radiative recombination rate and reducing the non-radiative recombination rate, the IQE optimization for InGaN QWs also require careful consideration of the current injection efficiency ($\eta_{Injection}$) for high current density operation.

It is widely observed that c-plane InGaN QW based LEDs suffer from the reduction in efficiency at high operating current density, i.e. "efficiency droop" [77]. Experimental studies show that the efficiency of the InGaN QW LEDs reaches peak value at low injection current (J~5-20 A/cm^2), which reduces as the injection current increases [77]. Up to date, the origin of this phenomenon is still controversial and inconclusive. Various possible explanations were proposed as the mechanisms for the efficiency droop in high current operated devices as follows: (1) carrier leakage [78,79], (2) large Auger recombination rate at high carrier density [80–82], (3) decreased carrier localization at In-rich regions at high injection densities [83], (4) hole transport impediment and consequent electron leakage [84,85], and (5) junction heating [86]. Kim, et al. and Schubert, et al. reported that the efficiency droop in InGaN QW LEDs was related to the recombination of carriers outside the MQW region [78,79]. Shen and associates reported a large Auger recombination coefficient (C_{Auger} ~1.4-2 x 10^{-30} cm^6/s) in InGaN materials [80]. However, the calculated Auger coefficient for direct Auger process indicated C_{Auger} ~10^{-34} cm^6/s [87]. Recent works based on first principle method indicated that the Auger coefficient in InGaN materials as C_{Auger} ~2 x 10^{-30} cm^6/s [80] and C_{Auger} ~3-4 x 10^{-31} cm^6/s [82], attributed to the interband Auger and indirect Auger processes, respectively. In addition, recent works by Chow and associates have also suggested the possibility of electron plasma heating in the QW as the primary carrier leakage mechanism [88]. Although it

#147902 - $15.00 USD
Received 19 May 2011; accepted 22 Jun 2011; published 1 Jul 2011
(C) 2011 OSA

is uncertain of the origin of the efficiency droop in InGaN QW LEDs, the carrier-dependent droop phenomenon is clear that leads to efficiency droop at high injection level.

Several possible solutions to address the efficiency droop have also been presented as follow: (1) the use of thicker InGaN active layer [89], (2) the use of polarization-matched barrier materials [78,79], and (3) the use of larger bandgap barrier materials [90–92]. The use of thicker InGaN active layer in LED devices have led to significantly lower carrier density in the active layer, which in turn leads to peak efficiency up to current density above 200 A/cm^2 [89]. The use of polarization-matched AlInGaN barrier material also enables the suppression of efficiency-droop in InGaN QW LEDs. An important consideration in the pursuit of the approaches to suppress efficiency droop in nitride LEDs is the growth compatibility in implementing the approach. An interesting approach to suppress or reduce the efficiency droop at high current density in InGaN QW LEDs is by employing thin lattice-matched $Al_{0.83}In_{0.17}N$ barrier layers [90] surrounding the InGaN QW active region [as shown in Fig. 15(a)]. As shown in Fig. 15(b), the use of thin AlInN barrier layers is expected to lead to efficiency-droop suppression up to high current density (J > 450 A/cm^2) [90]. Recently, Choi, et al. and Kim and associates reported significant improvement in the electroluminescence emission intensity in InGaN LEDs by employing the $In_{0.18}Al_{0.82}N$ electron block layer, which led to suppression of droop up to J ~200 A/cm^2 [91,92]. These findings indicated that the suppression of carrier leakage is crucial for reducing the efficiency droop in InGaN QWs [90–92], and optimizing the current injection efficiency is important for enabling high IQE devices at high current density.

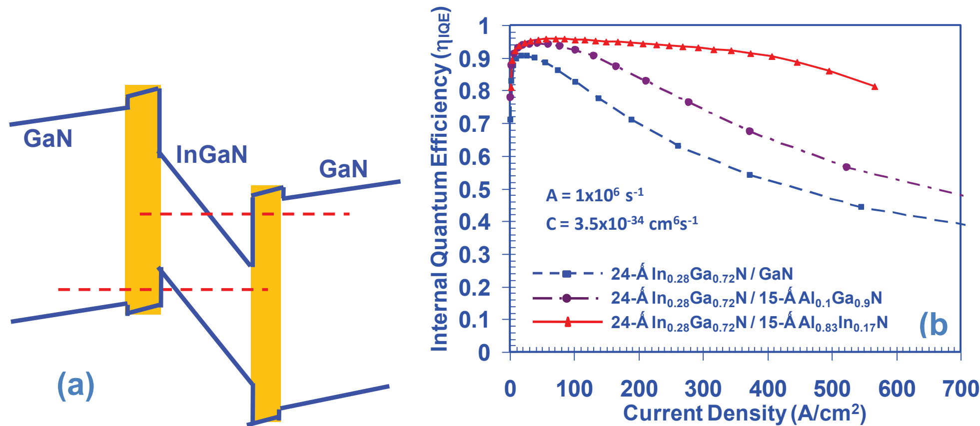

Fig. 15. (a) Schematic of the InGaN-GaN QW structure inserted with large bandgap barriers. (b) IQE (η_{IQE}) as a function of total current density for 24-Å $In_{0.28}Ga_{0.72}N$ / GaN QW, 24-Å $In_{0.28}Ga_{0.72}N$ / 15-Å $Al_{0.1}Ga_{0.9}N$ QW and 24-Å $In_{0.28}Ga_{0.72}N$ / 15-Å $Al_{0.83}In_{0.17}N$ QW.

7. Summary

In summary, the staggered InGaN QWs with enhanced radiative efficiency are analyzed as improved active region for LEDs application. Various issues related to the use of large overlap QWs for addressing low IQE in green spectral regime were reviewed. The less-abrupt interface in staggered InGaN QWs due to the graded growth temperature approach will not affect the performance of the staggered InGaN QWs detrimentally. The epitaxy of linearly-shaped staggered InGaN QWs was presented. The finding indicates that the use of LS staggered InGaN QWs can be relatively practically implemented by using graded growth temperature technique under current control mode. Other important issues in optimizing the IQE of InGaN QW LEDs related to defect reduction and efficiency droop suppression were discussed. The employment of thin large band gap barrier materials surrounding the InGaN QWs leads to significant enhancement of current injection efficiency, which suppresses the efficiency droop in III-Nitride LEDs. The optimization of both radiative efficiency and current

injection efficiency enables the realization of high internal quantum efficiency for nitride based LEDs emitting in the green wavelength region and longer.

Acknowledgments

The authors acknowledge supports from US National Science Foundation (Grant No. ECCS # 0701421, ECCS # 1028490), US Department of Energy (Grant No. DE-FC26-08NT01581), and Class of 1961 Professorship Funds. This manuscript is an invited journal paper as part of the Energy Express focus issue.